PNAS
www.pnas.org

Supplementary Information for

Cardiac myosin activation with 2-deoxy-ATP via increased electrostatic interactions with actin

Joseph D. Powers, Chen-Ching Yuan, Kimberly J. McCabe, Jason D. Murray, Matthew Carter Childers, Galina V. Flint, Farid Moussavi-Harami, Saffie Mohran, Romi Castillo, Carla Zuzek, Weikang Ma, Valerie Daggett, Andrew D. McCulloch, Thomas C. Irving, and Michael Regnier

Joseph D. Powers & Michael Regnier
Email: j2powers@ucsd.edu; mregnier@uw.edu

This PDF file includes:

Supplementary text
Figs. S1 to S2
Tables S1 to S2
References for SI reference citations

www.pnas.org/cgi/doi/10.1073/pnas.1905028116

Supplementary Information Text

Supplemental Methods

Animal use and ethics

All animal experiments were done in compliance with protocols approved by both the University of Washington and the Illinois Institute of Technology Institutional Animal Care and Use Committees and followed the "Guide for the Care and Use of Laboratory Animals" (National Research Council, 2011). Fourteen adult male Fischer 344 rats were used in the experiments. The rats were euthanized by carbon dioxide inhalation and exsanguination.

Heart excision and trabeculae preparation

Rat hearts were rapidly excised and perfused via retrograde flow through the aorta with room-temperature and oxygenated (95% O2 and 5% CO2) Kreb-Henseleit (KH) solutions containing (in mM) 118.5 NaCl, 5 KCl, 1.2 $MgSO_4$, 2 NaH_2PO_4, 25 $NaHCO_3$, 1.8 $CaCl_2$, 10 glucose, and 20 2,3-butanedione monoxime, (BDM; used to minimize damage during dissection). Papillary muscles and trabeculae were carefully dissected from the right ventricle and immediately placed in 'skinning' solution containing (in mM) 100 KCl, 10 MOPS, 5 EGTA, 9 $MgCl_2$ and either 1 mM dATP or 4 mM ATP (adjusted to pH = 7 with KOH), 1% (by volume) Triton X-100 and 1% protease inhibitor (Sigma P8340) at room temperature. The solution was replaced every 30-45 minutes and preparations were removed after 90-120 minutes of incubation in the skinning solution. Custom aluminum T-clips were placed on each end of the preparations to facilitate mounting them between a rigid post and a dual-action length/force transducer (Aurora Scientific 402A). Skinned muscle preparations were then washed 3 times with solution without TritonX-100 on ice. Skinned muscle bundles were transferred to 'resting solution' (pCa 9.0) containing either 2 mM dATP or ATP before X-ray experiments. Preparations were only ever in contact with ATP or dATP-containing solution once skinning had begun.

X-ray diffraction data collection

X-ray diffraction experiments used the small-angle instrument on the BioCAT beamline 18ID at the Advanced Photon Source, Argonne National Laboratory (1). X-ray focal spots were about 0.5 x 0.5 mm at the sample and 0.06 x 0.15 mm at the detector with a maximum incident flux of 10^{13} keV photons/s. To reduce radiation damage, the beam was attenuated (typically 10-fold) using aluminum attenuators. The sample-to-detector distance was 3 meters. Skinned muscle preparations were mounted in a custom mechanics rig allowing for simultaneous X-ray diffraction

and mechanics measurements. Fibers were mounted on a 500 mV force transducer (Model 402A, Aurora Scientific Inc.) and force was monitored by an ASI 610A data acquisition and control system. Solutions were changed using a syringe pump equipped with a multiway valve (Hamilton model 500). Sarcomere length was adjusted to ~2.0 μm using laser diffraction (or by adjusting the length such that the trabeculae is taut) and stretched by 15% to reach a length of 2.3 μm. Simultaneous force and diffraction pattern measurements were performed in pCa 9.0 and pCa 5.2 solutions. Diffraction patterns were collected only at the plateau phase of force development in activation pCa 5.2 solution. Small-angle X-ray diffraction patterns were collected on a CCD-based X-ray detector (Mar 165, Rayonix Inc. Evanston, IL). The instrument was calibrated using the 58.380 d_{001} peak of a silver behanate standard.

X-ray data analysis and statistics

The data were analyzed using data analysis programs belonging to the MuscleX software package (Version 1.13) developed at BioCAT (Jiratrakanvong et al., 2018). The lattice spacing and intensity ratios were measured using the "Equator" routine in MuscleX. The spacing and intensity of the M3 layer were measured using the "Diffraction Centroids" routine in MuscleX. The M3 intensity has been normalized with the total intensity of the estimated diffuse background generated by the "Quadrant fold" routine.

Computational structural analysis of actin-myosin complexes and Brownian dynamics simulations

A previous Molecular Dynamics study on pre-powerstroke myosin (PDB: 1VOM) yielded the starting structures for our myosin rigid bodies (2). PDB files for Run 1 of the MD simulations at the 50 ns timepoint with only protein present (no ligands) were used for both ADP-bound and dADP-bound myosin [the myosin structure equilibrated by 30 ns, as discussed in Nowakowski *et al.* (2)]. An actin monomer (PDB: 2ZWH) with all ligands removed was used to avoid interactions with other binding sites along the thin filament (3). The actin and myosin-(d)ADP structures were manually aligned using Visual Molecular Dynamics (VMD) to ensure that the myosin binding cleft on actin was appropriately oriented with the binding domain on myosin (4). To ensure the accuracy of the bound conformation, the actin monomer was aligned with Chain B of rigor myosin X co-complexed with actin (PDB: 5KG8) and the myosin structures were aligned with Chain A of the same PDB structure (5).

PQR files were generated for all structures using PDB: 2PQR (6). Electrostatic potential grids were generated using APBS version 1.4 by solving the Poisson-Boltzmann equation using the

AMBER force field at 300K (7). A relative permittivity of 4 was used for the solute, and 78.5 for the solvent, and a 150 mM concentration of KCl was assumed for the system. A list of polar complex pairs (defined as 'contact pairs') was generated by comparing the myosin and actin input coordinates and considering pairs of atoms within 3.5 Å of each other, and the complete list of contact pairs can be found in associated files. A total of 49 atom pairs met the criteria for the ADP case, and 66 atom pairs met the criteria for the dADP case.

Actin-myosin association simulations were performed using Browndye software to determine the differences between ATP- and dATP-bound myosin in terms of actin association kinetics (8). The myosin structures from the alignment analysis were used together with an actin dimer (two actin monomers using PDB: 2ZWH overlaid onto PDB: 5KG8) to simulate myosin association kinetics to the thin filament. A simulation trajectory was considered successful when at least 3 polar contact pairs were within the prescribed 'reaction distance' criterion, and association rates were determined by using the ratio of successful to unsuccessful trajectories together with the assumed diffusivity of the molecules (9). Specifically, the association rate constant (k_{on}) is calculated as

$$k_{on} = s \cdot k_{db} \cdot (a/n) \qquad \textit{Eq. S1}$$

where s is a scaling factor, a is the number of binding events, n is the total number of trajectories, and k_{db} is the rate constant of diffusion as calculated using the Smoluchowski equation (*i.e.*, the diffusion-limited case) using information about the molecule charges and solvent (9). The reaction distance criterion was varied to examine a large range of possible rates since experimental association rate data for this system are unavailable. 500,000 independent trajectories were performed to calculate the average association rates for both the ADP and dADP case to decrease the width of the binomial rate distribution and increase confidence in the rate calculations.

Energetic calculations for an actin-myosin complex

Energies were calculated for the bound actin-myosin complex using AMBER 18 (10). From the PDB file containing both actin and myosin, parameter/topology (prmtop) and coordinate/restart (inpcrd) files were created using tleap (a program within the AMBER suite that generates topology files from predetermined coordinate files) and AMBER protein forcefield ff14SB (11). Initially, the total energy was calculated in PMEMD (Particle Mesh Ewald Molecular Dynamics) using thermodynamic integration (ADP-Myosin: -2.96×10^4 kcal·mol^{-1}, dADP-Myosin: -3.2075×10^4 kcal·mol^{-1}). To ensure that atom overlap was not incorrectly affecting energy

calculations, 20,000 minimization steps were performed on the system using PMEMD. Minimization had little effect on the energetic calculations—after minimization, energies were calculated as -3.05×10^4 kcal·mol^{-1} for ADP-myosin and -3.25×10^4 kcal·mol^{-1} for dADP-myosin.

Allosteric effects of dATP in the nucleotide binding pocket

To investigate the mechanism by which the specific bound nucleotide altered allosteric communication between the nucleotide binding pocket and the actin binding surfaces, we analyzed our previously reported simulations of pre-powerstroke myosin from *Dictyostelium discoideum* (PDB ID: 1VOM) in the presence of P_i, Mg^{2+}, and either ADP or dADP (2). As previously reported, all-atom molecular dynamics simulations were performed using the *in lucem* molecular mechanics package (12, 13) the Levitt *et al.* force field (14), and explicit flexible 3-center water molecules (15). Simulations of the ADP and dADP systems were performed in triplicate for 50 ns each using the microcanonical ensemble (NVE, constant number of particles, **v**olume, and **e**nergy).

First, we analyzed contacts formed between the nucleotides and residues in the nucleotide binding pocket at the residue level (Figure S1). The nucleotides were considered in contact with a myosin residue if a pair of carbon atoms were separated by less than 5.4 Å or if a pair of noncarbon atoms were separated by less than 4.6 Å. This analysis considers whether at least one pair of myosin-nucleotide atoms were in contact, not the total number of atomic contacts formed with each specific residue. The first 10 ns of simulation time for each replicate was excluded from these calculations.

We found that the nucleotides interacted with V126, N127, P128, F129, S181, G182, A183, G184, K185, T186, and S236 for a similar fraction of the total simulation time (Figure S1A). This included most of the residues in the P-loop (residues 179-186), which anchors and orients the nucleotides in the binding pocket via interactions with the phosphate groups on ADP and dADP. Other residues within the nucleotide binding pocket interacted with ADP and dADP for distinct fractions of the simulation time (Figure S1B). Among others, ADP interacted with N233, N234, and N235 for a greater fraction of the simulation time than dADP. These residues are located in switch 1 (residues 233 – 240), which is thought to transmit structural changes from the nucleotide binding pocket to actin binding sites (16).

To investigate whether these altered interactions between switch 1 and either ADP or dADP propagated to other regions of myosin, we performed dynamic cross-correlation analysis of C_α atoms, which quantifies the extent to which the motions of different residues are correlated. Cross-correlations were calculated after the structural alignment of snapshots from the simulations taken at 1 ns intervals. After calculating the dynamic cross correlations for all pairs of C_α atoms,

we calculated the average cross-correlations between switch 1 residues and other residues in myosin (Figure S2). The cross-correlation analysis revealed several regions in myosin that had nucleotide-dependent correlations with switch 1: residues 355-440, which includes components of the upper 50 kDa domain and the O-helix; residues 460-500, which includes the relay helix; and residues 540-600, which includes components of the lower 50 kDa domain (indicated by the lower black lines in Figure S2).

Based on the results of our contact and cross correlation analyses, we propose that altered interactions between either ADP or dADP and switch 1 alter the dynamics of switch 1. Consequently, the distinct conformations of actin binding surfaces observed in the presence of dADP are the result of changes made to an allosteric pathway that connects the nucleotide binding pocket, switch 1, and the actin binding sites.

In-vitro motility assay

In-vitro motility (IVM) assays were performed as previously described (17). In brief, cardiac myosin was prepared from male Fisher rat ventricles by first adding extraction buffer (0.3 mM KCl, 0.15 mM Imidazole, 10 mM $Na_2P_2O_7$, 1 mM $MgCl_2$, 2 mM DTT) to minced ventricle tissue and stirring for approximately 30 minutes in a small beaker. Excess protein and residual actin were then removed by centrifugation for 1 hour with the supernatant then diluted 15-to-20-fold with water containing 2 mM DTT and left on ice for 1 hour to allow for myosin precipitation. Rat cardiac heavy meromyosin (HMM) was prepared by chymotryptic digestion (50 μg/ml) of myosin as described (18) and stored in -80°C for up to a week with 1% sucrose and 1% protease inhibitor (Sigma-Aldritch, St. Louis, MO). F-actin was prepared from rabbit skeletal muscle ether powder labeled with rhodamine-phalloidin (Invitrogen, USA) as previously described (18–20) and stored at 4°C and used within 6 weeks.

Flow cells were constructed from two glass cover slips separated by 2-mm foam adhesion strips with a total chamber volume of ~60 μL. The lower side surface was coated with 0.1% nitrocellulose in amyl-acetate (Sigma). Experimental procedure was similar to Gordon and colleagues (21). Briefly, isolated HMM (0.16 mM) in Buffer D solution (2 mM $MgCl_2$, 5 mM EGTA, 5 mM DTT, 10mM Imidazole, 0.2mM PMSF) was added to the flow cell for 3 minutes followed by bovine serum albumin (0.5 mg/mL BSA) in buffer (AB) (containing in mM, 25 KCl 25 imidazole, 4 MgCl2, 1 EGTA, and 1 DTT) to block nonspecific protein binding to the surface. This was then followed by an AB wash, addition of non-labeled sheared F-actin (1 μM) for 1 min, followed by another AB wash, and finally the addition of 0.5 mM ATP in AB. This was followed by another AB wash and RhPh F-actin was then added for 1 minute, finally followed by the

experimental motility buffer. The motility buffer consisted of AB buffer with 2 mM (d)ATP, 18 μg/ml catalase, 0.1 mg/ml glucose oxidase, 3 mg/ml d-glucose, and 40 mM DTT to minimize photooxidation and photobleaching. Ionic strength was varied from 50 to 130 mM with KCl. Variation in ionic strength depended on volume percentage of 2 M KCL, with 0% at IS 50 and linearly increasing by 0.005% per 10 mM of IS. All motility assays were performed at 30 ± 1°C. Each experimental slide was analyzed in at least six different regions, with the recording set for 10 seconds, each at 10Hz with IVM Image Acquisition. Recordings were then analyzed digitally, using a custom software developed by our laboratory that allows for filament counting and tracking.

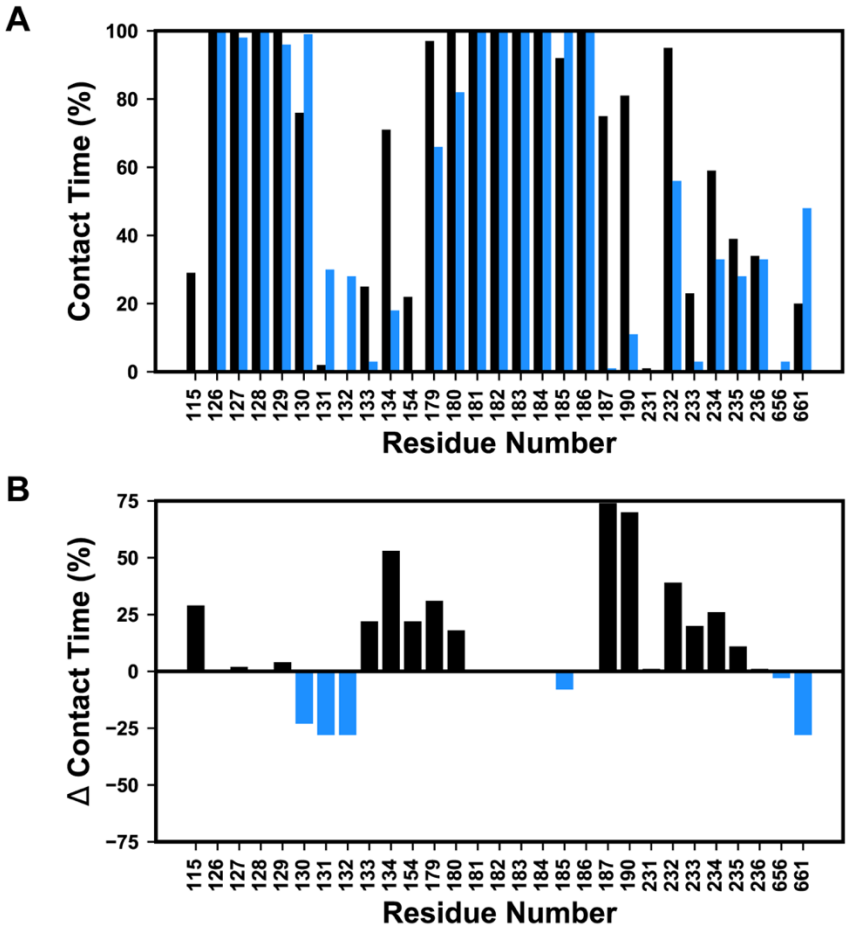

Figure S1. ADP and dADP form distinct sets of contacts within the nucleotide binding pocket. (A) The average percentage of simulation time that residues in the nucleotide binding pocket interacted with ADP (black bars) or dADP (blue bars). (B) The difference in the percentage of simulation time that specific residues interacted with either ADP or dADP highlights sets of residues that form distinct sets of interactions in the two systems. Black bars with positive values indicate that those residues interacted with ADP for a greater percentage of the simulations and blue bars with negative values indicate residues that preferentially interacted with dADP.

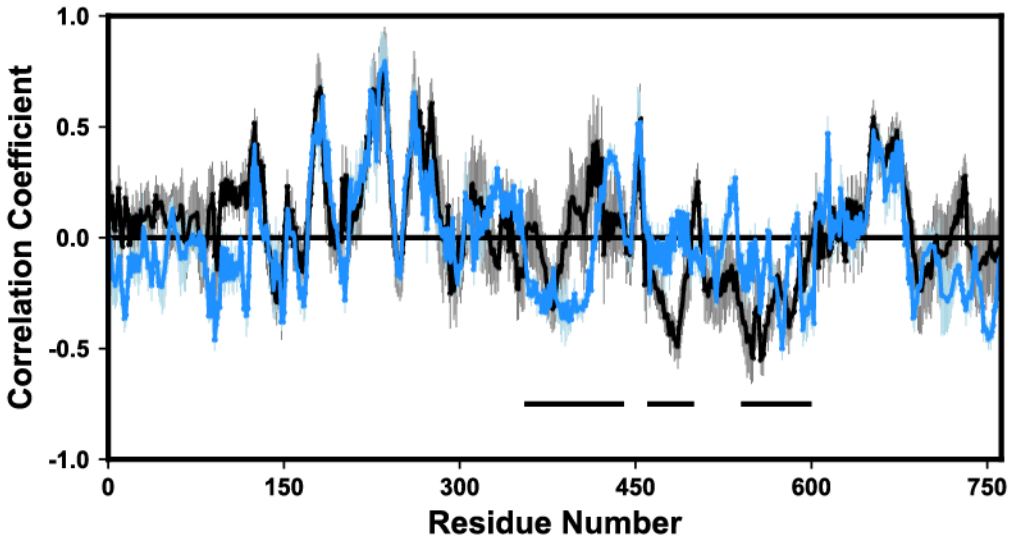

Figure S2. ADP and dADP induce distinct dynamics in switch 1. We averaged the cross-correlation coefficients for all residues in switch 1 (residues 233 – 240). Thin error bars denote the standard deviation of the correlation coefficients within this loop. Many regions of myosin, including most of the N-terminal domain had similar correlation coefficients with switch 1 in the presence of ADP (black) and dADP (blue). However, there were several regions, including residues 355-440, 460-500, and 540-600 that had nucleotide-dependent correlations with switch 1 (indicated be the black lines).

Supplemental Tables

Table S1. Numerical values of X-ray diffraction reflections of relaxing muscle (pCa 9.0).

X-ray Reflection	SL = 2.0 μm			
	μ = 170 mM		μ = 100 mM	
	ATP	dATP	ATP	dATP
$d_{1,0}$ (nm)	42.25 ± 0.36	41.29 ± 0.24*	38.77 ± 0.23	39.26 ± 0.20
$I_{1,1}/I_{1,0}$	0.38 ± 0.03	0.51 ± 0.05*	0.28 ± 0.03	0.35 ± 0.03
S_{M3} (nm)	14.42 ± 0.03	14.54 ± 0.02*	14.37 ± 0.01	14.40 ± 0.01
I_{M3} (a.u.)	3.95 ± 0.30	3.98 ± 0.42	5.07 ± 0.43	5.19 ± 0.38

X-ray Reflection	SL 2.3 μm			
	μ = 170 mM		μ = 100 mM	
	ATP	dATP	ATP	dATP
$d_{1,0}$ (nm)	38.02 ± 0.21	38.88 ± 0.34*	37.33 ± 0.69	37.28 ± 0.93
$I_{1,1}/I_{1,0}$	0.30 ± 0.03	0.43 ± 0.05*	0.33 ± 0.04	0.42 ± 0.05
S_{M3} (nm)	14.37 ± 0.01	14.42 ± 0.02*	14.39 ± 0.04	14.40 ± 0.04
I_{M3} (a.u.)	4.90 ± 0.49	4.97 ± 0.33	5.45 ± 0.45	5.20 ± 0.44

Values represent mean ± S.E.M. for $n > 14$ preparations. *$p<0.05$ comparing ATP to dATP using an unpaired student t-test.

Table S2. Quantification of X-ray diffraction reflections in resting and activated cardiac muscle with ATP or dATP.

X-ray Reflection	ATP		dATP	
	pCa 9.0	pCa 5.2	pCa 9.0	pCa 5.2
$d_{1,0}$ (nm)	38.02 ± 0.20	39.22 ± 0.46*	38.86 ± 0.33	39.04 ± 0.32
$I_{1,1}/I_{1,0}$	0.30 ± 0.03	0.52 ± 0.05*	0.43 ± 0.05	0.61 ± 0.07*
S_{M3} (nm)	14.37 ± 0.01	14.47 ± 0.04	14.42 ± 0.02	14.47 ± 0.03
I_{M3} (a.u.)	4.90 ± 0.49	3.88 ± 0.39*	4.97 ± 0.33	4.42 ± 0.40

SL = 2.3 μm; μ = 170 mM; Values represent mean ± S.E.M. for $n > 8$ preparations; *$p < 0.05$ using a paired t-test within nucleotide groups across pCa. Data for each nucleotide at pCa 9.0 are the same as Table S1 for SL 2.3 μm and μ = 170 mM, shown again here for clarity.

References

1. Fischetti R, et al. (2004) The BioCat undulator beamline 18ID: A facility for biological non-crystalline diffraction and X-ray absorption spectroscopy at the Advanced Photon Source. *J Synchrotron Radiat* 11(5):399–405.
2. Nowakowski SG, Regnier M, Daggett V (2017) Molecular mechanisms underlying deoxy-ADP.Pi activation of pre-powerstroke myosin. *Protein Sci* 26(4):749–762.
3. Oda T, Iwasa M, Aihara T, Maéda Y, Narita A (2009) The nature of the globular- to fibrous-actin transition. *Nature* 457(7228):441–445.
4. Humphrey W, Dalke A, Schulten K (1996) VMD: Visual Molecular Graphics. *J Mol Graph* 14(1):33–38.
5. Ropars V, et al. (2016) The myosin X motor is optimized for movement on actin bundles. *Nat Commun* 7. doi:10.1038/ncomms12456.
6. Dolinsky TJ, Nielsen JE, McCammon JA, Baker NA (2004) PDB2PQR: An automated pipeline for the setup of Poisson-Boltzmann electrostatics calculations. *Nucleic Acids Res* 32(WEB SERVER ISS.):665–667.
7. Baker NA, Sept D, Joseph S, Holst MJ, McCammon JA (2001) Electrostatics of nanosystems: Application to microtubules and the ribosome. *Proc Natl Acad Sci* 98(18):10037–10041.
8. Huber GA, McCammon JA (2010) Browndye: A Software Package for Brownian Dynamics. *Comput Phys Commun* 118(11):1896–1905.
9. Luty BA, McCammon JA, Zhou HX (1992) Diffusive reaction rates from Brownian dynamics simulations: Replacing the outer cutoff surface by an analytical treatment. *J Chem Phys* 97(8):5682–5686.
10. Case DA, et al. (2018) AMBER 2018. *Univeristy California, San Fr*.
11. Maier JA, et al. (2015) ff14SB: Improving the Accuracy of Protein Side Chain and Backbone Parameters from ff99SB. *J Chem Theory Comput* 11(8):3696–3713.
12. Beck DAC, McCully ME, Alonso DO V., Daggett V in lucem molecular mechanics (ilmm). *Univ Washington; Seattle*:2000–2019.

13. Childers MC, Daggett V (2018) Validating Molecular Dynamics Simulations against Experimental Observables in Light of Underlying Conformational Ensembles. *J Phys Chem B* 122(26):6673–6689.

14. Levitt M, Hirshberg M, Sharon R, Daggett V (1995) Potential energy function and parameters for simulations of the molecular dynamics of proteins and nucleic acids in solution. *Comput Phys Commun* 91(1–3):215–231.

15. Levitt M, Hirshberg M, Sharon R, Laidig KE, Daggett V (1997) Calibration and Testing of a Water Model for Simulation of the Molecular Dynamics of Proteins and Nucleic Acids in Solution. *J Phys Chem B* 101(25):5051–5061.

16. Kuhner S, Fischer S (2011) Structural mechanism of the ATP-induced dissociation of rigor myosin from actin. *Proc Natl Acad Sci* 108(19):7793–7798.

17. Razumova M V., et al. (2006) Effects of the N-terminal domains of myosin binding protein-C in an in vitro motility assay: Evidence for long-lived cross-bridges. *J Biol Chem* 281(47):35846–35854.

18. Kron SJ, Toyoshima YY, Uyeda TQP, Spudich JABT-M in E (1991) Assays for actin sliding movement over myosin-coated surfaces. *Molecular Motors and the Cytoskeleton* (Academic Press), pp 399–416.

19. Pardee JD, Aspudich J (1982) Purification of Muscle Actin. *Methods Enzymol* 85(C):164–181.

20. Spudich JA, et al. (1982) Actin and myosin: control of filament assembly. *Philos Trans R Soc Lond B Biol Sci* 299(1095):247–261.

21. Gordon AM, LaMadrid MA, Chen Y, Luo Z, Chase PB (1997) Calcium regulation of skeletal muscle thin filament motility in vitro. *Biophys J* 72(3):1295–1307.